J Solid State Electrochem (2009) 13:231–238
DOI 10.1007/s10008-008-0549-8

ORIGINAL PAPER

Paramagnetic pyrrole-based semiconductor molecular material

Mathieu Lazerges · Kathleen Isabelle Chane-Ching · Salah Aeiyach · Saloua Chelli · Brigitte Peppin-Donnat · Martial Billon · Christian Lombard · François Maurel · Mohamed Jouini

Received: 30 September 2007 / Revised: 4 February 2008 / Accepted: 6 February 2008 / Published online: 22 April 2008

Abstract The electrochemical oxidation of hexa-*N*-pyrrolylbenzene in organic media leads, via intramolecular coupling of the pyrrole residues, to the deposition of a molecular semiconductor film on an electrode surface. In situ electron spin resonance–electrochemical experiments reveal that the semiconductor is endowed with both properties of conducting polymers (i.e., reversible oxidation) and polyaromatic molecular materials (i.e., highly paramagnetic). The material, which is easy to process as soft homogeneous thin film, shows a tunable 0 to 1 spin concentration per molecule at room temperature by controlling the electrochemical potential.

Keywords Organic semiconductor · Polyaromatic · Electrochemistry · ESR

Contribution to the Fall Meeting of the European Materials Research Society, Symposium D: 9th International Symposium on the Electrochemical–Chemical Reactivity of Metastable Materials, Warsaw, 17th–21st September, 2007.

K. I. Chane-Ching · S. Aeiyach · S. Chelli · F. Maurel · M. Jouini (✉)
ITODYS, Université Denis Diderot CNRS UMR 7086,
1 rue Guy de la Brosse,
75005 Paris, France
e-mail: jouini@univ-paris-diderot.fr

B. Peppin-Donnat · M. Billon · C. Lombard
DRFMC/SPrAM,
Université Joseph Fourier CEA CNRS UMR 5819,
17 Avenue des Martyrs,
38054 Grenoble, France

M. Lazerges
Laboratoire Génie Analytique, EA 4131 CNAM,
292 rue Saint Martin,
75003 Paris, France

Introduction

Organic conjugated materials are extensively investigated because they combine electronic properties of semiconductor and metals to the ease of processing of organic matter. One major challenge of these materials is to improve electronic properties, especially in magnetism, as these materials have a great potential to design ferromagnets [1], supraconductors [2], or flexible radio frequency shielding coatings [3]. Both polyaromatic hydrocarbons (PAHs), like graphite [4] or coronene [5], and conducting polymers (CPs), such as polyaniline [6] or polyacethylene [7], show magnetic behaviors. However, CPs are generally less paramagnetic than radical molecular compounds because of the spin recombination at oxidized state. We established recently that oxidation of hexa-*N*-pyrolbenzene **(A)** gives rise to formation of the polyheterocyclic compound **(B)** [8] through coupling of the six-pyrrole residues [9] (Fig. 1a) with a consequent formation of an organic semiconductor as a result of aggregation of **(B)**. This material includes aromatic cycle such as coronene and hexapyrrole chain and, hence, consists of both the PAH and CP families. We report in this paper thin layer electrosynthesis and characterization of this material and elucidation of radical formation process by in situ electrochemical–electron spin resonance (ESR) measurements.

Experimental

Commercial compounds Hexafluorobenzene (Aldrich, reagent grade), pyrrole (Acros, reagent grade), $LiClO_4$ (Acros, spectroscopic grade), and CH_3CN (Merck, spectroscopic grade) were used without further purification.

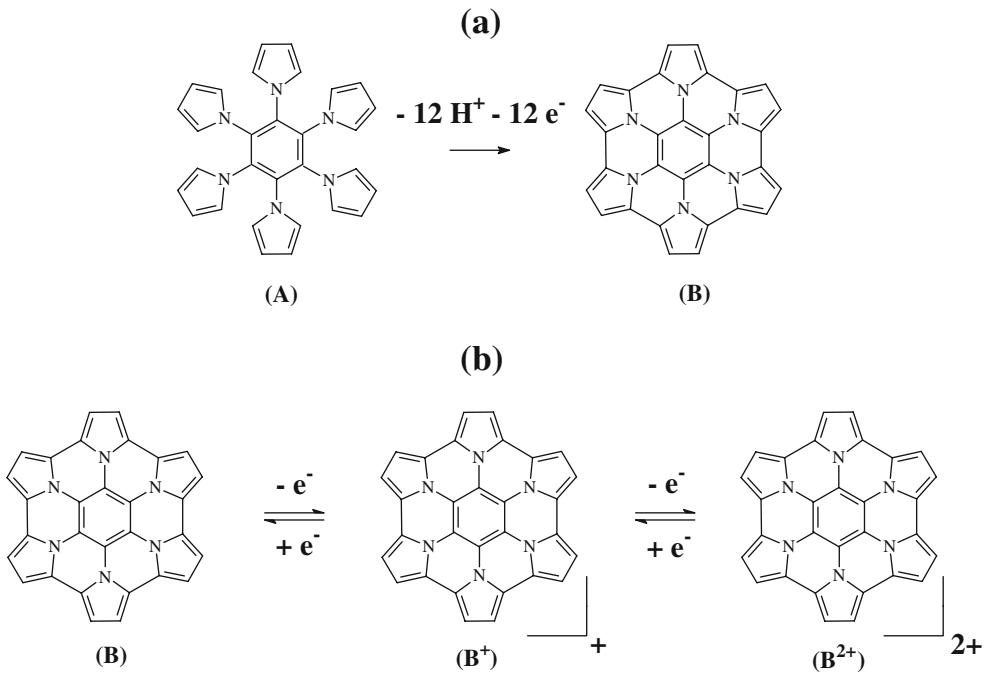

Fig. 1 **a** Electrosynthesis of molecular material **(B)** from compound **(A)**, **b** reversible oxidation process of **(B)** to cation **(B^+)** and divalent cation **(B^{2+})**

Chemical synthesis The synthesis of compound **(A)** was performed in 93% yield by adaptation of a previously described procedure [10]. The product was purified by crystallization. $C_{30}H_{24}N_6$; chemical analysis C 76.7 (76.92), H 5.4 (5.13), N 17.9 (17.94); Matrix-assisted laser desorption–ionization-time-of-flight mass spectrometry (*m*/*z*) 468.57 (468.56) ($M^{\bullet+}$); ^{1}H NMR ($CDCl_3$) δ 6.08 (12H, t, *J*=2.2 Hz), δ 6.18 (12H, t, *J*=2.2 Hz); ^{13}C NMR ($CDCl_3$) 110.6 (−), 120.8 (+), 134.2 (+).

Electrochemical Experiments were driven in one-compartment three-electrode cell with an 'EG&G PAR 373A' potentiostat. The electrochemical potentials are reported versus saturated calomel electrode (SCE) and electrochemical kinetics was given in current density (A cm^{-2}). The sweep rate for voltammetry experiments was 100 mV s^{-1}. The electrolyte was 0.1 M $LiClO_4$ in CH_3CN. **(A)** was used at a 10^{-3} M concentration for electrochemical film synthesis.

Electrochemical set-up for electrochemical synthesis, electrochemical activity, SEM, FTIR, and XPS analysis The solutions were argon deaerated prior to electrochemical experiments. The working electrodes were indium tin oxide (ITO) thin film on glass (1.87 cm^2) for electrochemical synthesis and activity and platinum (about 1 cm^2) for scanning electron microscopic (SEM), X-ray photoelectron spectroscopy (XPS), and Fourier transform infrared spectroscopy (FTIR) analysis. The counter-electrode was stainless steel grid, and the reference electrode was SCE with a salt bridge containing the electrolyte.

In situ electrochemical–electronic absorption analysis A film synthesized ex situ using previous conditions on an ITO electrode (about 1 cm^2) was rinsed with a CH_3CN solution and immersed in a quartz optical cell which contained the electrolyte. The counter-electrode was a platinum wire and the reference electrode an Ag/AgCl wire. The film was disposed through the 1 cm path of a ultraviolet (UV)-visible-near-IR 'VARIAN CARY 500' spectrometer and connected to the potentiostat to perform electronic in situ absorption measurements from UV to near-infrared regions at oxidized states.

In situ electrochemical–ESR analysis The electrolyte was nitrogen deaerated prior to electrochemical experiments. ESR–electrochemical experiments were performed in a one-compartment three-electrode cell. The working electrode was a platinum wire (0.42 cm^2), the counter-electrode a platinum plate and the reference electrode an Ag wire covered with AgCl immersing in a CH_3CN salt bridge containing 10^{-2} M $AgNO_3$. Spectra were recorded on an ER 200D SRC Bruker spectrometer.

Conductivity Conductivity measurements were performed on a SOLARTRON 1260 Schlumberger.

XPS XPS signals were recorded obtained using a VG ScientiÐc ESCALAB MKI system operating in the constant analyzer energy mode, "advantage software" version 2.20 was used for digital acquisition and data processing. An Mg–Kα X-ray source was used and the pass energy was set at 50 eV. The pressure in the analysis chamber was 10^{-9} mbar.

Calculations Geometry calculations were performed with the DFT B3LYP/6–31G(d) method and frequency calculations with Spartan AM1 method.

Results and discussion

Electrochemical synthesis The cyclic voltammograms of a solution of **(A)** during repeated scans between 0 and 1.20 V on ITO electrode shows an irreversible oxidation peak foot at 1.20 V. Two reversible oxidation waves which increase during cycling appear at 0.3 and 0.7 V (Fig. 2a). At the same time, the ITO electrode becomes brown. We showed in a previous paper that the irreversible electrooxidation process results from pyrrole α–α' intramolecular coupling [9] (Fig. 1) and leads to an insoluble product (**B**). The progressive coloration of the electrode and the growth of the two waves are attributed to the deposition of an electroactive conducting film produced by (**B**) aggregation on the electrode. The same results are obtained on a platinum electrode. Electrical conductivity of the film in the doped state measured in ambient atmosphere with the four-point contact method was 10^{-5} S cm^{-1}. The SEM photo of a film electrodeposited on a platinum plate during 40 scans between 0 and 1.20 V in (**A**) solution is presented in Fig. 3. The thickness determined using SEM after scratching the film with a surgeon scalpel is close to 150 nm. The upper part of the figure is the surface of deposit, and the lower part is the platinum surface on which the deposited film has been removed. The middle dark region corresponds to the cross section of the deposit. This photo indicates that the metallic substrate is covered by a homogeneous thin film. The organic thin film was not soluble in aqueous medium (acidic, basic, or neutral) nor in usual organic ones (CH_3CN, hexane, *N*-methylpyrrolidone, dimethylformamide, tetrahydrofuran). This is also the case for compounds which have extended π-conjugated structures similar to (**B**), like polyaromatic hydrocarbons found in coal tar [11] or those obtained from mild Lewis acid oxidation of oligophenylenes [12, 13] and from solid-state carbonization of pitch [5, 14].

XPS analysis The XPS spectrum of a film electrodeposited on a platinum plate electrode during 20 scans between 0 to 1.2 V in (**A**) solution is presented in Fig. 4. The peaks analyzed were as follows [15–18]: Cl_{2p} (208.3 eV), C_{1s} (286 eV), N_{1S} (401.9 eV) O_{1S} (533.0 eV), O_{KLL} Auger peak (981 eV). The 208.3 eV energy Cl peak value

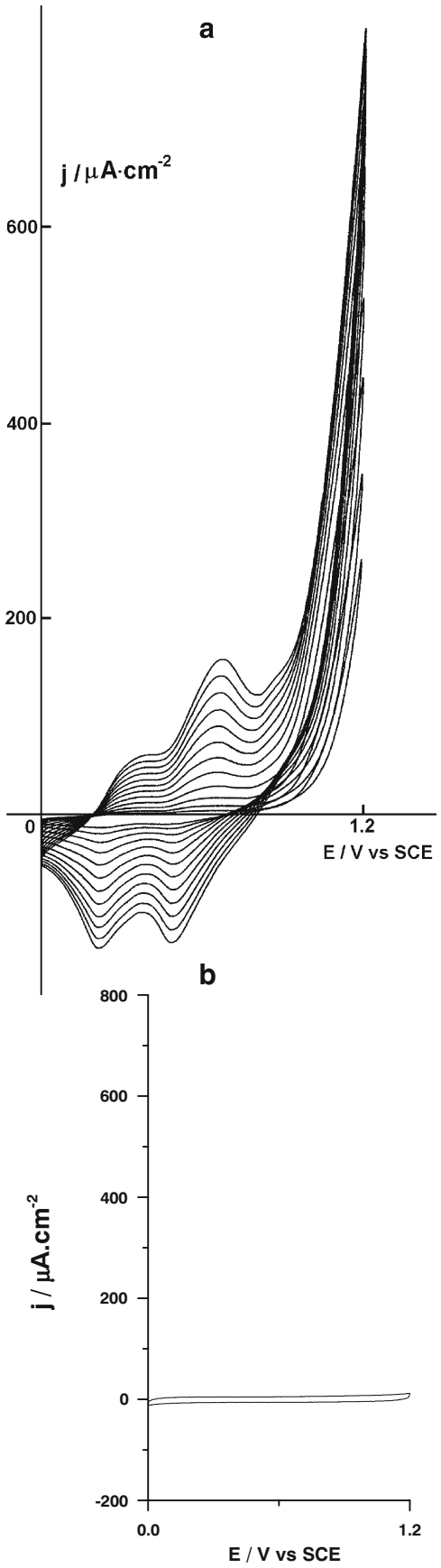

Fig. 2 Cyclic voltammetry experiments on an ITO electrode at 100 mv/s sweep rate in 0.1 M $LiClO_4$ CH_3CN electrolyte, **a** electrochemical synthesis of molecule material **(B)** from compound **(A)** at a 10^{-3} M concentration, (**b**) electrolyte background

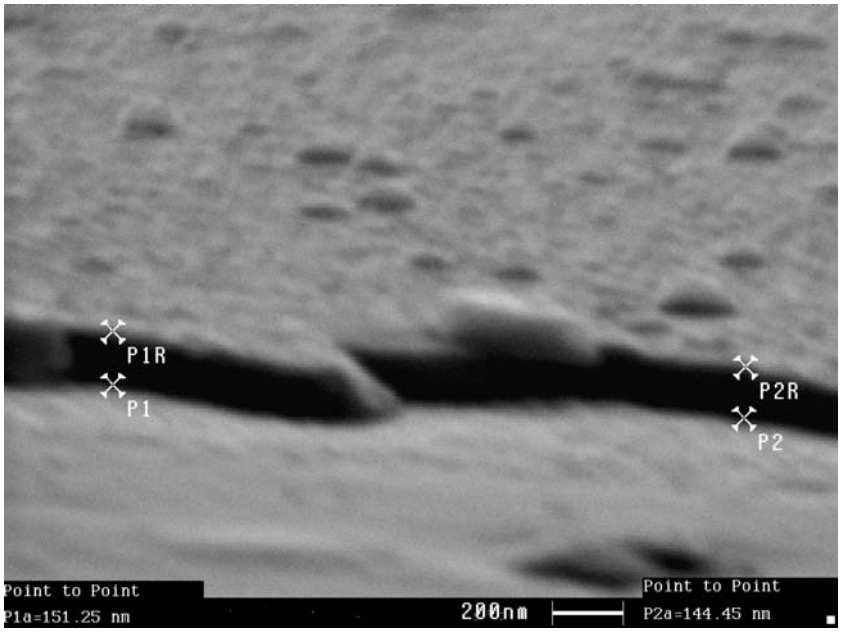

Fig. 3 SEM photo of a material thin film obtained from electrochemical synthesis on a platinum plate

indicates that this element is combined in ClO_4^- [19]. The peak area integrations lead to the following composition (C 71%, N 12%, O 13%, Cl 3%), which yield to the molecular formula $C_{30}N_6(ClO_4)_{1.4}$. This formula corresponds to **(B)** doped with 1.4 ClO_4^- anions (C 70%, N 14%, O 13%, Cl 3%). The material doping level per pyrrole unit is close to 0.23. This value is higher than 0.15 found for poly-*N*-phenyl-pyrrole and lower than 0.25–0.30 found for polypyrrole [20]. The low doping level in poly-*N*-phenyl-pyrrole was attributed to the perpendicular position of the phenyl residues against the polymer chain which in this position twists the polymer chain and prevents electron delocalization. Consequently doping process is also partially prevented when compared to unsubstituted polypyrrole. In our material, the doping level is intermediate, and, therefore, we can suggest that delocalization is also partially prevented. Oxidized films remain stable under air, but the surface of neutral films is rapidly oxidized.

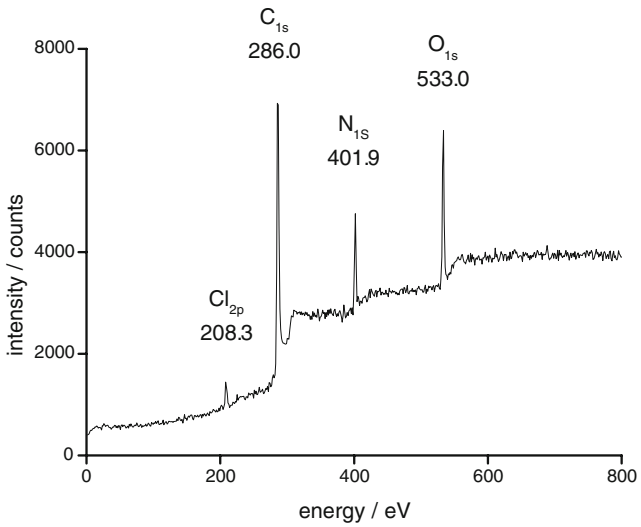

Fig. 4 XPS spectrum of the film material obtained from electrochemical synthesis on a platinum plate

FTIR analysis The infrared spectrum of 1 wt.% **(A)** in KBr is shown in Fig. 5a. A film was electrodeposited on platinum plate during 20 cycles between 0 and 1.20 V in a solution of **(A)**. This film was reduced in the same medium to a neutral state by application of a −0.5 V potential during 10 min, and an infrared analysis was performed ex situ under nitrogen atmosphere. Another film was electrodeposited using the same procedure and was oxidized by application of a 0.8 V potential in the same electrolytic medium without **(A)** during 10 min and an infrared analysis was performed ex situ. The infrared spectra of the neutral and the oxidized films are presented in Fig. 5b. The bands at 3.106, 3.120, 3.130, and 3.140 cm^{-1} are attributed to C–H pyrrole stretching vibrations. Before **(A)** oxidation, the band at 727 cm^{-1} is attributed to C–H_β pyrrole bending vibration [21, 22]. After oxidation, **(B)** is formed and a new band at 770 cm^{-1} is attributed to the same C–H_β pyrrole bending vibration when there is no hydrogen in α position. The vibration band at 1,680 cm^{-1} that does not exist in **(A)** spectrum is attributed to the formation of a pyrazin ring after intramolecular pyrrole coupling. The stretching vibration of a pyrazin ring occurs at 1,590 cm^{-1} [23, 24]. The calculated geometry of the **(B)** molecule is curved, as shown in Fig. 6. The calculated pyrazin fragment stretching vibration for this curved geometry is 1,665 cm^{-1}. This calculated value is

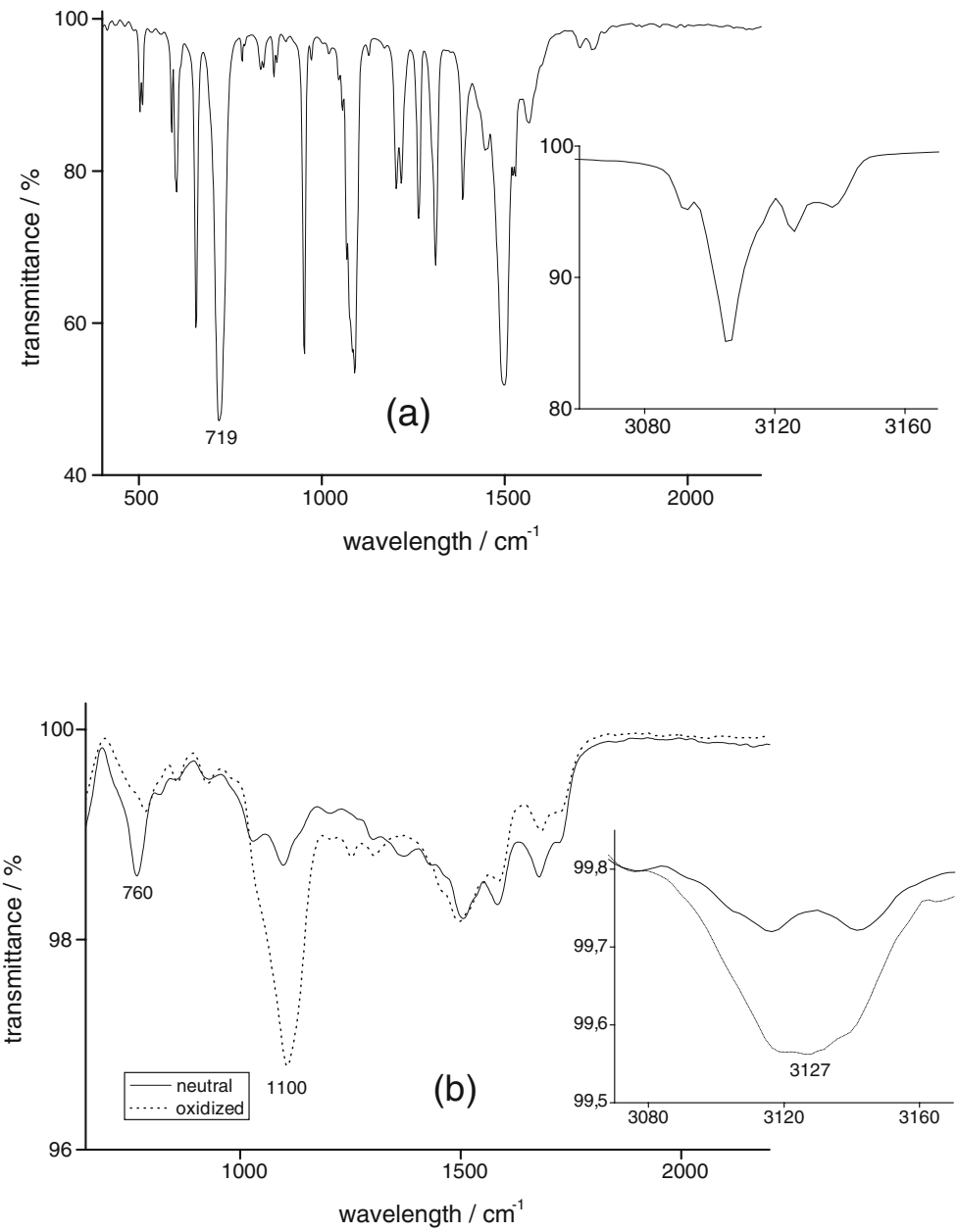

Fig. 5 **a** IR spectrum of the compound **(A)** at 1% in KBr, **b** FTIR spectra of the film material **(B)** obtained from electrochemical synthesis on a platinum plate at the neutral and oxidized states

close to our 1,680 cm^{-1} experimental value. This curved shape in **(B)** induces cycle tension of pyrazin fragment that explains the high frequency of this band. A similar curved geometry was found for corannulene, which is induced by the presence of a five-membered ring centered among six-membered rings [25]. The band at 1,099 cm^{-1} in the spectrum of the film at oxidized state is attributed to the Cl–O stretching vibration of ClO_4^-. This band disappears in the spectrum of the film in neutral state, indicating that the doping process is reversible.

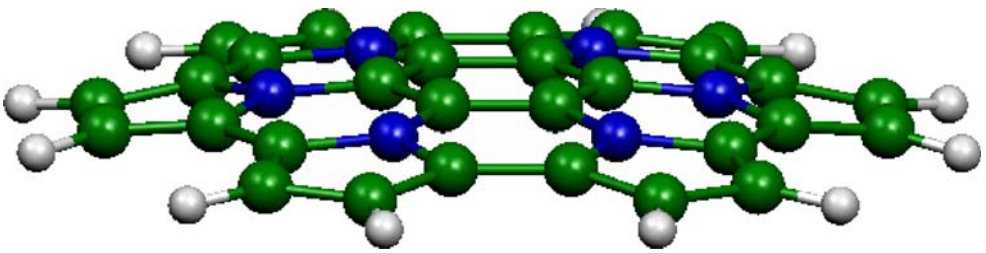

Fig. 6 Calculated geometry of the material molecule **(B)** with DFT B3LYP/6–31G(d) method

Electrochemical reversible oxidation The film prepared as indicated in Fig. 2 was rinsed with CH_3CN and immersed in CH_3CN containing 0.1M $LiClO_4$. Cyclic voltammetry between 0 and 0.8 V shows two well-separated and reversible waves (Fig. 7a). The mean value, corresponding to the oxidation and reduction peak potentials of each reversible redox process, are located at 0.30 and 0.53 V. The charges under each wave deduced from integration are equal to each other, indicating successive oxidation of (**B**) to the cation ($\mathbf{B}^+$) and divalent cation ($\mathbf{B}^{2+}$; Fig. 1b). The mean value of the oxidation peak potentials is of 0.46 V. This value is close to the 0.45 V peak potential of poly (*N*-phenyl-pyrrole) oxidation [20]. This means that the charge in the organic material constituted of disk-like molecules which posses a ring of six-pyrroles and a benzene center is as well stabilized as a linear-conducting *N*-phenyl-substituted polypyrrole.

ESR–electrochemical analysis The thin film was synthesized in a 10^{-3} M **(A)** electrolyte at 1.2 V for 5 min. The

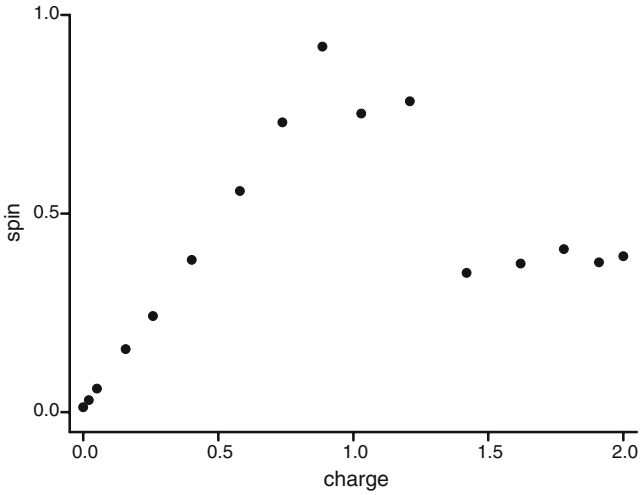

Fig. 8 Spin versus charge curve of the material film **(B)** obtained from in situ ESR electrochemical experiments

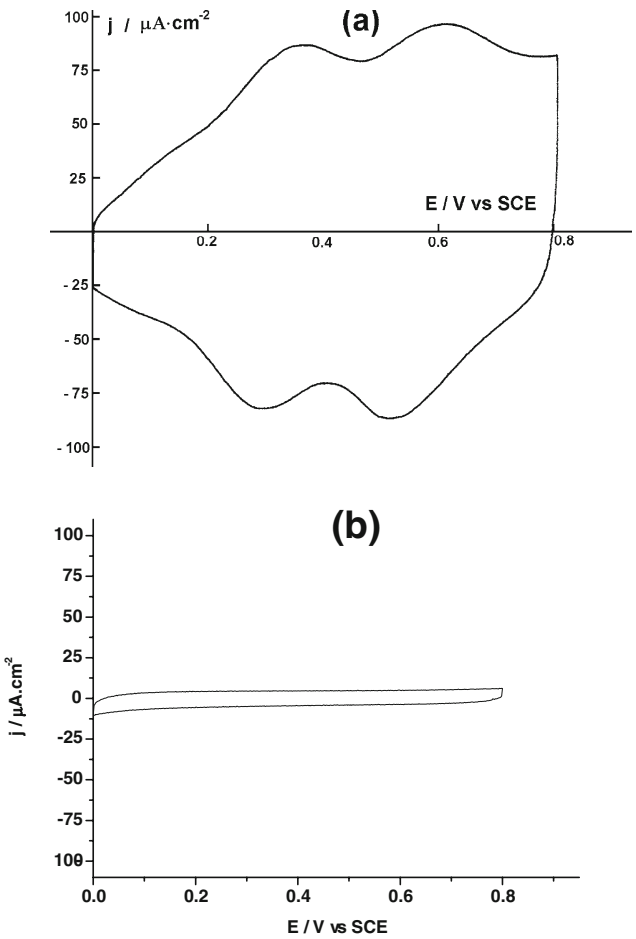

Fig. 7 Cyclic voltammetry experiments on an ITO electrode at 100 mv/s sweep rate in 0.1 M $LiClO_4$ CH_3CN electrolyte, **a** electrochemical activity of material film **(B)**, **b** electrolyte background

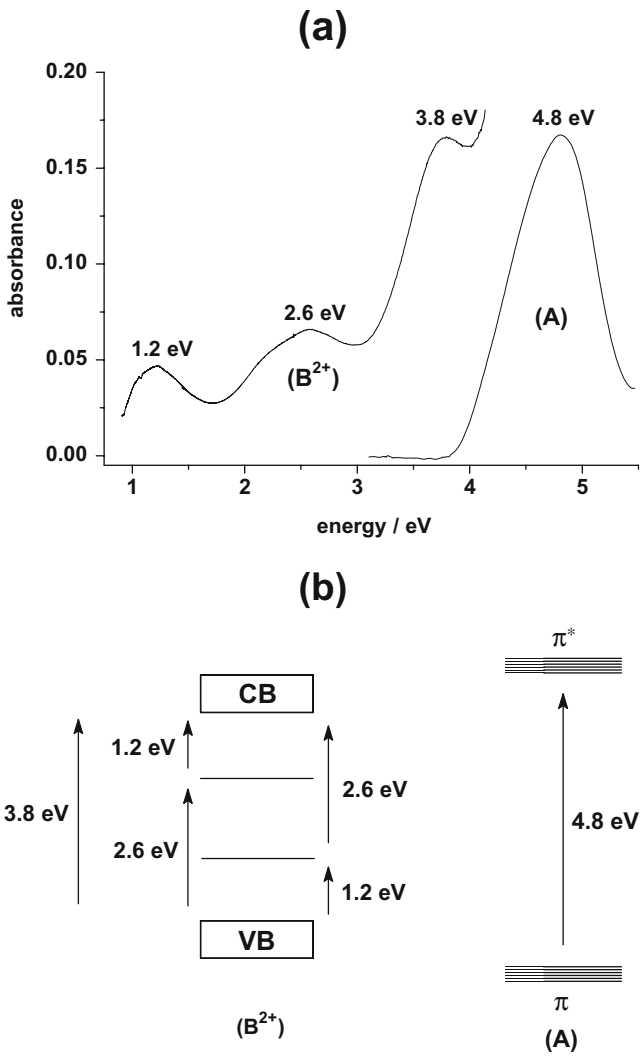

Fig. 9 **a** Electronic absorption spectrum in CH_3CN of compound **(A)** at a 10^{-3} M concentration and material **(B)**, **b** corresponding energy diagrams

working electrode wire coated with this organic electroactive thin film was transferred in an electrochemical cell adapted for ESR measurements. The cell was filled with 1 M $LiClO_4$ in CH_3CN. The cell was introduced into the magnetic field of an ESR spectrometer operating at 9 GHz (X band). The film spin concentration was measured from neutral state (**B**) to divalent cation state ($\mathbf{B^{2+}}$) by applying a constant potential during 3 min at each 50 mV step between 0 and 0.8 V. The spin versus positive charge curve is presented in Fig. 8. The same curve was obtained for the oxidation as well as for the reduction sweeping, indicating a reversible spin formation process. The first part of the curve is linear, from 0 to 1 positive charge injected (R^2=0.997), indicating that one spin is formed for each positive charge injected in the film. It means that (**B**) is oxidized to the radical cation ($\mathbf{B^{+}}$) at first. This behavior is fundamentally different from polypyrrole where recombination process between radical cations occurs at earlier stage less than one injected charge amount. For a charge injection greater than one, the molecular spin density decreases, indicating oxidation of the radical ($\mathbf{B^{+}}$) to the divalent cation ($\mathbf{B^{2+}}$). Nevertheless, a population of radicals remain for two positive charges transferred per molecule. This spin population may be constituted of both radical ($\mathbf{B^{2+}}$) and diradical ($\mathbf{B^{2+}}$) divalent cations. Both intrarecombination and interrecombination processes can occur, yielding respectively to the formation of bipolarons [26, 27] and π-dimers [28–31]. It is important to note that the spin density found close to one is higher than the spin density of the higher paramagnetic CPs, where the maximum spin density measured on polypyrrole is 0.8 per hexapyrrole unit [32]. Moreover, the population of spins remaining at the oxidized state is in opposition to polypyrrole where the spin is equal to zero consecutively to recombination processes. This paramagnetic behavior in terms of high spin density and diradical existence is similar to that of molecular compounds which possess similar sixfold symmetric axis like coronene [33], hexaaminobenzene derivatives [34, 35] and hexamethoxytriphenylene [36].

Electronic absorption analysis The electronic absorption of **(A)** measured in acetonitrile shows a peak at 4.8 eV (Fig. 9a). The electronic absorption of an organic material film electrodeposited on ITO was measured from UV to near-infrared regions (Fig. 9a). The spectrum shows three absorption peaks located at 1.2, 2.6, and 3.8 eV. The **(A)** and **(B)** absorption maxima, located at 4.8 and 3.8 eV, respectively, are attributed to π–π* transitions. The **(A)** oxidation leads to **(B)**, which is a polyheteroaromatic compound with delocalized electrons. Therefore, the **(B)** π–π* transition at 3.8 eV is lower than the **(A)** π–π* transition at 4.8 eV. Moreover, the energy of the π–π* transition at 3.8 eV is equal to the sum of the transition energies at 2.6 and 1.2 eV. Taking into account this equality, we attribute these two peaks to transitions involving two energy states of cationic charge carriers in the gap (Fig. 9b). Such electronic diagram including energy states in the gap is similar to those of linear-conducting polymers.

Conclusion

The electrochemical oxidation of a sixfold *N*-pyrrolyl-substituted benzene star-shaped conjugated molecule leads to the deposition of a thin film of an organic semiconductor material. SEM photo reveals a homogeneous film structure. XPS and IR analyses indicate that it is constituted of π-conjugated molecules that include a six-pyrrole ring. This structure is very different from those of organic semiconductors classically obtained from pyrrole derivatives which are linear polymers. The electrochemical behavior shows two oxidation waves attributed to the successive formation of cation and divalent cation species versus one single large oxidation wave for polypyrrole. In situ ESR measurements show that the first electron transfer corresponds to the formation of paramagnetic cation–radical species, contrary to conducting polymers where recombination process between radicals occurs. This material shows a remarkable magnetic behavior, corresponding to one spin per six-pyrrole ring versus 0.8 per six-pyrrole linear unit in the most paramagnetic conducting polypyrrole. This high spin density in the material is similar to the spin density measured in radical organic salts like hexaaminobenzene derivatives. The energy diagrams deduced by electronic absorption measurements of the material at the oxidized state, reveals energy states in the gap as it is the case for conducting polymers. In conclusion, this physical–chemistry study reveals that the semiconductor obtained is endowed with both properties of conducting polymers (i.e. reversible oxidation, easy to process as thin film) and polyaromatic molecular materials (i.e. highly paramagnetic).

Acknowledgement This work was supported by fellowship for Dr. Mathieu Lazerges from the 'Ministère de l'Education et de la Recherche Française'. The authors thank Pr. Kacem Zellama (Laboratoire de Physique de la Matière Condensée, Université de Picardie Jules Verne) for conductivity measurements, Dr. Jean-Claude Blais (Laboratoire de Chimie Structurale Organique et Biologique, Université Paris VI Pierre et Marie Curie) for MALDI TOF analysis, Dr. Alain Adenier (ITODYS, Université Paris VII Denis Diderot) for FTIR measurements, Dr. Mehdi Chehimi (ITODYS, Université Paris VII Denis Diderot) for XPS measurements, Stephan Borensztajn (Laboratoire Interfaces et Systèmes Electrochimiques, Université Paris VI Pierre et Marie Curie) for SEM photos, Dr. John Sydney Lomas, Dr. Gilles Horowitz (ITODYS, Université Paris VII Denis Diderot) and Monique Lecomte (Laboratoire Génie Analytique, CNAM Paris) for fruitful discussions.

References

1. Takahashi M, Turek P, Nakazawa Y, Tamura M, Nozawa K, Shiomi D, Ishikawa M, Kinoshita M (1991) Phys Rev Lett 67:746
2. Jérôme D, Mazaud A, Ribault M, Bechgaard K (1980) J Phys Lett (Paris) 41:L–95
3. Dhawan SK, Singh N, Venkatachalam S (2002) Synth Met 125:389
4. Freise EJ (1962) Nature 191:671
5. Zander M, Collin G (1992) Fuel 72:1281
6. Doriomedoff M, Cristofini FH, Surville RD, Jozefowicz M, Yu LT, Buvet R (1971) J Chim Phys 68:1055
7. Chiang CK, Fincher CR, Park YW, Heeger AJ, Shirakawa H, Louis EJ, Gau SC, Diarmid AGM (1977) Phys Rev Lett 39:1098
8. Vegh D, Hrnciarikova K, Zalupsky P, Skakalova V, Fedorko P, Cik G (1997) 22nd Conference on Advances in Organic Chemistry. Papiernicka, Slovak Republic, pp 11–13 May
9. Lazerges M, Jouini M, Hapiot P, Guiriec P, Lacaze PC (2003) J. Phys. Chem. A. 107:5042
10. Biemans HAM, Zhang C, Smith P, Kooijman H, Smeets WJJ, Spek AL, Meijer EW (1996) J Org Chem 61:9012
11. Bäumler E (1989) Farben, Formeln, Forscher Hoechst und die Geschichte der industriellen Chemie. Riper, Munich
12. Clar E, Mackay CC (1972) Tetrahedron 28:6041
13. Müller M, Kübel C, Müllen K (1998) Chem Eur J 36:833
14. Boenigk W, Haenel MW (1995) Fuel 74:305
15. Beamson G, Briggs D (1992) High Resolution of Organic Polymers. Wiley, Chichester
16. Moulder JF, Stickle WF, Sobol PE, Bomben KD (1992) Handbook of X-ray Photoelectron Spectroscopy. PERKIN-Elmer, Minnesota
17. Robinson JW (1991) Practical Handbook of Spectroscopy. CRC, London
18. Briggs D, Seah MP (1990) Practical Surface Analysis, 2nd edn. Wiley, Chichester
19. Dall'Olio A, Dascola Y, Varacca C, Bocchi V (1968) C. R. Acad Sci Ser C 267:433
20. Diaz AF, Castillo J, Kanazawa KK, Logan JA, Salmon M, Fajardo O (1982) J Electroanal Chem 133:233
21. Scott DW (1971) J Mol Spectrosc 37:77
22. Acevedo-Gonzales CA, Campos-Valletté M, Clavijo-Campos RE (1986) Spectrochim Acta 42A:919
23. Lord RC, Marston AL, Miller FA (1957) Spectrochim Acta 9:113
24. Simmons JD, Innes KK, Begun G (1964) J Mol Spectrosc 14:190
25. Seiders TJ, Baldridge KK, Grube GH, Siegel JS (2001) J Am Chem Soc 123:517
26. Fichou D, Horowitz G, Garnier F (1990) Synth Met 39:125
27. Brédas JL, Street GB (1985) Acc Chem Res 18:309
28. Miller LL, Tu Y, Esmir G, Duan R (1995) Adv Mat 5:547
29. Scott JC, Pfluger P, Krounbi MT, Street GB (1983) Phys Rev B 28:2140
30. Bäuerle P, Segelbacher U, Gaudl KU, Huttenlocher D, Mehring M (1993) Angew Chem Int Ed Engl 32:76
31. Haare JAEHV, Groenendaal L, Having EE, Janssen RAJ, Meijer EW (1996) Angew Chem Int Ed Engl 35:638
32. Genou F, Guglielmi M, Nechtschein M, Genies E, Salmon M (1985) Phys Rev Lett 55:118
33. Krusik PJ, Wasserman E (1991) J Am Chem Soc 113:2322
34. Breslow R, Maslak P, Thomaides JS (1984) J Am Chem Soc 106:6453
35. Lepage TJ, Breslow R (1987) J Am Chem Soc 109:6412
36. Bechgaard K, Parker VD (1972) J Am Chem Soc 94:4749